Two-dimensional imaging of CF_2 density by laser-induced fluorescence in CF_4 etching plasmas in the gaseous electronics conference reference cell

Brian K. McMillin[a] and Michael R. Zachariah[b]

Chemical Science and Technology Laboratory, National Institute of Standards and Technology, Gaithersburg, Maryland 20899

Spatially resolved two-dimensional maps of the relative CF_2 density in low-pressure radio-frequency $Ar/CF_4/O_2$ discharges generated within a parallel-plate Gaseous Electronics Conference reference cell have been obtained using planar laser-induced fluorescence imaging. The experiments cover a wide range of pressure, composition, flow rate, and power deposition conditions (13.3–133.3 Pa, 1%–100% CF_4, 1%–10% O_2, 5–100 sccm, 3–35 W). Typically, the centerline ($r = 0$) axial CF_2 distribution was symmetric with the local peak occurring near the center of the electrode gap, but, in all cases, significant radial variations in CF_2 density were observed (14%–45% standard deviation from the mean) with the peak density occurring near the edge of the discharge region. Varying the pressure led to significant changes in both the magnitude and spatial distribution of CF_2 density, while varying the composition, flow rate, and power primarily affected only the magnitude of the CF_2 density, with only modest changes in the spatial distribution. Based on image-averaged comparisons, the CF_2 density increased with power, pressure, and CF_4 mole fraction, decreased with addition of oxygen, and varied nonmonotonically with flow rate. [S0734-2101(97)03302-2]

I. INTRODUCTION

Low-pressure radio-frequency (rf) plasma etching of silicon dioxide with CF_4-based chemistries is used extensively during the manufacturing of microelectronic integrated circuits.[1,2] Despite their widespread use, the physical and chemical phenomena which determine the behavior and the resulting etching performance of these plasmas are not fully understood. With regard to the gas-phase chemistry, for example, a great deal of experimental[1,2] and, to a lesser extent, modeling research[2] as been conducted to improve the understanding of these plasmas, but detailed comparisons between modeling and experiment have been limited. Species measurements have been made by a number of techniques, but typically these have been limited to single-point, line-of-sight, or one-dimensional (1D) spatial profile measurements within the glow region of the plasma. As two-dimensional (2D) modeling becomes more widespread, a more extensive experimental data base will be necessary for benchmarking and verification of these plasma chemistry models.

In previous studies, we used planar laser-induced fluorescence (PLIF) imaging to map the argon metastable density field in low-pressure argon and argon/molecular discharges.[3–4] The purpose of this study is to extend those PLIF measurements to map the spatially resolved, 2D CF_2 density field in $Ar/CF_4/O_2$ etching plasmas generated within a Gaseous Electronics Conference (GEC) rf parallel-plate

reference cell.[5] The CF_2 radical is an important species in halocarbon plasmas because it influences the balance between polymer deposition and etching, and hence selectivity, in silicon/silicon dioxide etching applications.[1,2] As a result, a number of previous experimental studies have reported 1D measurements of CF_2 density using mass spectrometry,[6] infrared diode laser-absorption,[7–10] and laser-induced fluorescence,[11–19] but, to our knowledge, the present results are the first complete 2D measurements of CF_2 density in any reactor. In addition to yielding information on the relative magnitude of CF_2 concentration at various conditions, these measurements are of interest because they provide insight into the plasma uniformity through 2D visualization of the CF_2 spatial distribution. These detailed spatial distributions, which were obtained from the well-defined GEC cell reactor, should provide a useful data source for validation of multidimensional models.

In the following paragraphs, we briefly describe the experimental setup and then present contour maps of the spatially resolved CF_2 concentration as a function of power, feed gas composition, flow rate, and pressure in $CF_4/O_2/Ar$ plasmas. In addition, we examine the axially averaged and image-averaged measurements for a number of cases to illustrate the large-scale changes in the radial distribution and overall magnitude of the CF_2 concentration. For completeness, we also report results of a Fourier analysis of electrical measurements obtained during these experiments, including the amplitude of the voltage and current wave forms and their relative phase difference, the dc self-bias voltage, and the power deposited into the plasma.

[a]National Research Council NIST postdoctoral research associate, 1993–1995. Current address: Lam Research Corporation, 4650 Cushing Parkway, Fremont, CA 94538; Electronic mail: brian.mcmillin@lamrc.com
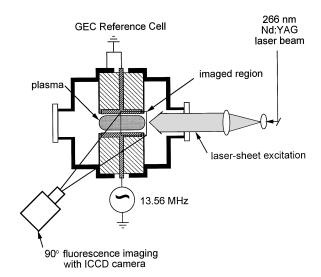[b]Electronic mail: mrz@tiber.nist.gov

FIG. 1. Schematic diagram of the experimental setup.

II. EXPERIMENTAL DETAILS

The experiments were conducted using a capacitively coupled, parallel-plate, asymmetrically driven GEC cell, which has been described in detail previously[5] and is shown schematically in Fig. 1. Briefly, the stainless steel reactor used here has 10.2-cm-diam aluminum water-cooled electrodes with a 2.25 cm separation. The lower electrode was powered with a 13.56 MHz supply coupled through a matching network and isolating rf filter. The upper electrode and the chamber were grounded. Voltage and current wave forms were measured with probes located at the base of the powered electrode (after the matching network) using a digitizing oscilloscope, and saved to a laboratory computer for later analysis. To determine the actual voltage, current, and power supplied to the plasma, these measured wave forms were Fourier analyzed and corrected for cell parasitics.[20]

The feed gas mixture is introduced through the upper electrode via a showerhead arrangement of holes. The feed gas then flows radially and symmetrically out of the discharge region and is removed from the chamber via a feedback-controlled throttle valve and mechanical pump. During these experiments, the flowrate was varied over 5–100 sccm and the pressure was varied over 13.3–133.3 Pa (100–1000 mTorr).

Spatially resolved 2D images of CF$_2$ relative concentration were obtained using PLIF imaging. The experimental setup and technique are similar to our previous studies,[3,4] so we only briefly describe review the details here; for additional information on LIF measurements in glow discharges and PLIF imaging in general, we refer the reader to Refs. 21 and 22, respectively. In this study, a quadrupled Nd:YAG laser sheet (266 nm, 10 ns, $\sim$0.3 mJ, $\sim$1 cm^{-1}, 5 mm$\times$25 mm) was used to illuminate the central vertical plane of the discharge and excite transitions in the $A(0,2,0)\leftarrow X(0,1,0)$ band[23] of CF$_2$. The resulting broadband laser-induced fluorescence (300–400 nm) was imaged at a 90° angle to the

illumination plane with an intensifier-gated, cooled CCD camera using an $f/4.5$ lens (see Fig. 1).

While acquiring images, a 300 nm long-pass filter was used to reject laser scattering and a colored-glass filter was used to reduce the visible plasma emission reaching the camera. The CF$_2$ fluorescence images were obtained by temporally averaging $\sim$1000 laser shots with an $\sim$300 ns intensifier gate width, and spatially averaging over 2$\times$2 pixels to improve the signal-to-noise ratio. The imaged region included approximately one-half of the discharge, extending from the centerline to $\sim$1 cm beyond the right edge of the electrodes. The spatial resolution of these measurements was determined by the laser sheet thickness ($\sim$5 mm) and the imaged dimensions of the camera pixels in the object plane ($\sim$0.2$\times$0.2 mm).

In reducing the raw fluorescence data, the plasma emission was first subtracted and then the images were normalized for spatial variations in laser energy and detector response. No corrections for fluorescence yield were necessary, because, as in previous studies,[12] no significant differences in the fluorescence decay time were observed for the conditions examined here. The fact that no quenching corrections were necessary here indicates that the spontaneous emission rate dominates the electronic quenching rate of CF$_2$ (for the major species in the plasmas examined here, i.e., Ar and CF$_4$), which is consistent with the rate coefficients available in the literature.[23–25]

In relating the fluorescence signal to the CF$_2$ density, [CF$_2$], the neutral gas temperature was assumed to be uniform, rotationally and vibrationally equilibrated, and constant for all conditions examined; i.e., we assumed the concentration of the laser-probed states inferred from the fluorescence measurement perfectly tracks the total CF$_2$ density. We estimate that neglecting the temperature dependence of the fluorescence signal results in a 10%–15% total ($\pm$5%–7.5%) uncertainty in the CF$_2$ density over the expected temperature range of 300$<T<$400 K for the plasmas examined here. This estimated uncertainty is based on Boltzmann population fraction calculations for the states probed by the 266 nm laser, which indicate that the fluorescence signal will increase with temperature; i.e., for a given CF$_2$ density the signal will be 10%–15% higher at 400 K than at 300 K.

III. RESULTS AND DISCUSSION

Relative 2D measurements of the CF$_2$ density distribution were obtained in Ar/CF$_4$/O$_2$ rf discharges over a wide range of pressure, composition, flow rate, and power deposition conditions (13.3–133 Pa, 1%–100% CF$_4$, 1%–10% O$_2$, 5–100 sccm, 3–35 W). While the absolute CF$_2$ density was not determined in these experiments, a recent investigation using a GEC cell[10] reported CF$_2$ densities of $\sim$10^{12}–10^{13} cm^{-3} in CF$_4$/CHF$_3$ plasmas at similar conditions. Generally speaking, in the present experiments, varying the pressure led to significant changes in both the magnitude and spatial distribution of CF$_2$ density, while varying the composition,

flow rate, and power led to pronounced changes in the magnitude with more subtle changes in the spatial distribution of CF_2 density.

As observed in previous GEC cell experiments,[3,4] significant radial variations in species concentration were observed (see, for example, Fig. 2). The peak CF_2 density typically occurs at $r \sim 3-5$ cm, near the edge of the powered electrode. Indeed, in almost all cases, the CF_2 concentration contours appear to attach to the corner of the powered electrode. The increased CF_2 (and presumably F) concentration near the edge of the powered electrode likely results from an increase in the electron impact production of CF_2, brought about by an enhanced electric field associated with the sharp external corner[26] of the electrode. This edge effect could potentially be reduced or eliminated by smoothing or reducing the exposure of the sharp corner on the powered electrode. Such edge effects have been recently examined in a different parallel-plate reactor geometry by comparing measured oxide etch rates and modeled ion flux profiles with various powered electrode configurations.[27]

For all of the cases examined here, the centerline ($r=0$) axial distribution of CF_2 density is relatively symmetric, with the peak occurring near the center of the discharge ($z \sim 1$ cm). This axial distribution largely reflects the CF_2 production profile, which is dominated[28] by the high energy electron impact reaction $e + CF_4 \rightarrow CF_2 + 2F + e$ (threshold ~ 13 eV). This is evidenced to some extent by the similarity of the present axial CF_2 profiles and previously reported argon emission profiles in Ar/CF_4 discharges at similar conditions,[4] since the argon excitation threshold (~ 13.5 eV) and cross-section energy dependence (over $\sim 12-30$ eV) are similar to those of the CF_4 electron impact reaction noted above (see, for example, Refs. 29 and 30). The CF_2 profile is, of course, also affected by diffusion, since CF_2 is a relatively long-lived species, and by destruction mechanisms such as heterogeneous (wall recombination) and gas-phase recombination reactions.[16]

A. Effect of power

Figure 2 shows contour plots of the spatial distribution of $[CF_2]$ in 75%CF_4/Ar discharges at 66.7 Pa (500 mTorr) and a 25 sccm flow rate at the lowest and highest powers examined here, 3.5 and 35 W, respectively. In these and all of the contour plots which follow, the $z=0$ and $z=2.25$ cm locations correspond to the powered and grounded electrodes, respectively. As power is increased over this range, the peak CF_2 concentration increases by more than an order of magnitude, and the edge-to-center concentration ratio increases. This change in radial nonuniformity is illustrated more clearly in Fig. 3(a), which shows the normalized radial $[CF_2]$ profiles averaged over the lower half of the discharge region adjacent to the powered electrode, i.e., averaged over $0 < z < 1.2$ cm. As indicated by the standard deviation from the mean, σ, the radial nonuniformity in $[CF_2]$ increases from 15%–34% as power is increased from 3.5–35 W. Aside from this increase in radial nonuniformity and a slight shift in the axial peak, though, we observe no significant change in the spatial distribution of CF_2 as the power is increased.
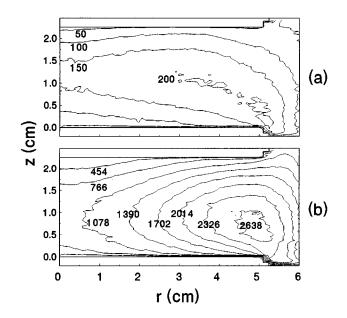

FIG. 2. Contour plots of the spatially resolved relative CF_2 density measured with laser-induced fluorescence in a 75%CF_4/Ar discharge at 25 sccm, 66.7 Pa (500 mTorr) and powers of (a) 3.5 and (b) 35 W.
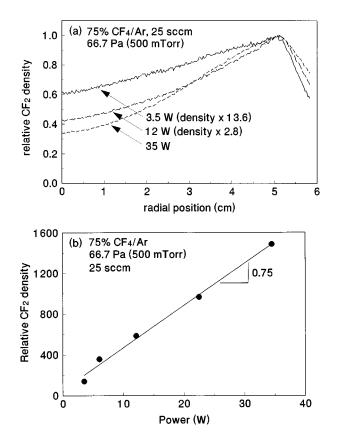

FIG. 3. (a) Axially averaged ($0 < z < 1.2$ cm) radial profiles of CF_2 density and (b) image-averaged CF_2 concentration as a function of power, determined from PLIF images of 75%CF_4/Ar discharges at 25 sccm and 66.7 Pa (500 mTorr). The radial nonuniformity of $[CF_2]$ in (a), as indicated by the standard deviation from the mean, σ, is 15%, 27%, and 34% for 3.5, 12, and 35 W cases, respectively. The normalized slope indicated in (b) denotes that the $[CF_2]$ increases by 7.5× as the power is increased by 10×.
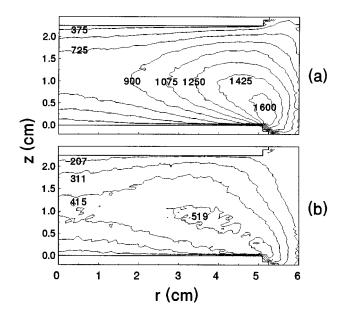
FIG. 4. Contour plots of the spatially resolved relative CF_2 density measured with laser-induced fluorescence in 25 sccm, 66.7 Pa (500 mTorr), 20 W discharges with feed gas compositions of (a) 75%CF_4/Ar and (b) 75% CF_4/10%O_2/Ar.

Figure 3(b), which shows the image-averaged $[CF_2]$, illustrates the change in the overall CF_2 concentration as a function of power. The $[CF_2]$ increases in an essentially linear fashion over the power range examined here, with a *normalized* slope of less than unity, where we define a *normalized* slope as the ratio of the fractional change in $[CF_2]$ to the fractional change in the parameter varied. The normalized slope of 0.75 denoted in Fig. 3(b) indicates that the $[CF_2]$ increases by 7.5× as the power is increased by 10×. The linear increase in $[CF_2]$ with power we observe is consistent with results reported by Pang and Brueck,[12] who measured the $[CF_2]$ ~3 mm above the powered electrode in a different reactor using single-point LIF; however, their measurements showed a more significant rate of increase in $[CF_2]$ with power (with a normalized slope as we have defined of ~1.3).

B. Effect of feed gas composition

The effect of feed gas composition on the CF_2 concentration was examined at fixed power, pressure and flow rate (20 W, 66.7 Pa, 25 sccm) by diluting the CF_4 feed gas with argon, and by adding O_2 to a baseline mixture. In the former cases, the CF_4 concentration was varied from ~1%–100%, and, in the latter cases, the mixtures were composed of 75% CF_4 and 1%–10%O_2 with a balance of argon. Figures 4(a)–4(b) show representative contour plots of $[CF_2]$ for 75%CF_4/Ar and 75%CF_4/10%O_2/Ar mixtures, which illustrate that varying the feed gas composition has only a modest effect on the spatial distribution of CF_2.

The effect of feed gas composition on the magnitude of $[CF_2]$ is illustrated in Figs. 5(a)–5(b) where the image-averaged $[CF_2]$ is shown as a function of CF_4 and O_2 percentage, respectively. As the concentration of CF_4 in the feed gas is increased from 1%–100%, the average CF_2 concentra-
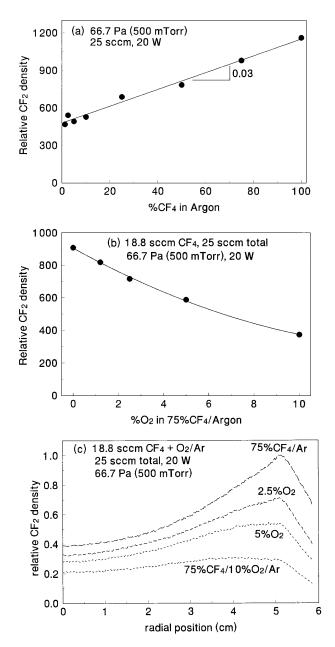

FIG. 5. Image-averaged CF_2 density as a function of (a) CF_4 and (b) O_2 mole fraction in the feed gas for 25 sccm, 66.7 Pa (500 mTorr), 20 W CF_4/O_2/Ar discharges, and (c) axially averaged ($0 < z < 1.2$ cm) radial profiles of CF_2 density for selected mixtures (σ=32%, 26%, 22%, and 16% for 0%, 2.5%, 5%, and 10% O_2, respectively). The normalized slope indicated in (a) denotes that the $[CF_2]$ increases by ~3× as the concentration of CF_4 in the feed gas is increased by 100×.

tion increases linearly by about 2.5×. An increase in CF_2 concentration is expected, because the electron impact production of CF_2 is proportional to the CF_4 feed gas concentration. However, this relatively weak increase in $[CF_2]$ suggests that very little of the CF_4 is dissociated in the pure CF_4 discharge at these conditions. For example, even if all of the CF_4 were dissociated for the most dilute (1.2% CF_4) case, the degree of dissociation for the pure CF_4 case can only be 2%–3%, since the primary fragments in the electron impact dissociation of CF_4 are CF_2 and CF_3 in a ~2.5:1 ratio.[28] This

relatively weak increase in the CF_2 concentration (and thus CF_4 dissociation) as the argon dilution is decreased may be due to the cooling of the high energy tail in the electron energy distribution and/or a decreased electron number density resulting from additional electron attachment by CF_4.

The effect of the addition of O_2 on the image-averaged $[CF_2]$ in the discharge is shown in Fig. 5(b). For these cases, the power was held constant at 20 W, and the CF_4 mole fraction and the total flow rate were held constant at 75% and 25 sccm, respectively. Here we observe a reduction in CF_2 density of about $2.5\times$ with 10% O_2 added to the feed gas, which is in good agreement with previous studies.[12,16] It is well established that the addition of oxygen can substantially reduce the CF_2 concentration, and this trend has been previously attributed to the radical exchange reactions with atomic oxygen, $CF_2+O \rightarrow COF+F$ and $CF_2+O \rightarrow CO+2F$.[28]

With regard to $[CF_2]$ spatial distribution, the various CF_4/Ar discharge mixtures were very similar, aside from the overall increase in $[CF_2]$ with increased CF_4 concentration in the feed gas. With the addition of oxygen, however, we observed a somewhat larger decrease in $[CF_2]$ near the edge of the discharge as compared to the center, leading to a more uniform radial distribution of CF_2. These trends are illustrated in Fig. 5(c), which shows representative axially averaged ($0 < z < 1.2$ cm) radial profiles of the normalized $[CF_2]$ for several feed gas mixtures; note, for example, $\sigma = 32\%$ and 16% for mixtures with 0% and 10% O_2, respectively. The larger decrease in $[CF_2]$ near the edge of the discharge (compared to $r=0$) with added oxygen may result, in part, from increased oxidation losses there. Although the rates for the oxidation reactions noted above would be higher near the edge of the electrode simply because the $[CF_2]$ is higher there, the larger fractional decrease in $[CF_2]$ (i.e., the decrease in $[CF_2]$ for the cases with added O_2 normalized by $[CF_2]$ for the baseline mixture) suggests that the atomic oxygen concentration is larger near the edge of the discharge as well. Such an enhancement in the atomic oxygen concentration near the edge of the discharge may result from an increase in electron impact dissociation of O_2 due to the enhanced electric field there. As discussed below, the more uniform radial distribution with added oxygen may also be due, in part, to more uniform CF_2 production associated with a more resistive plasma bulk.

C. Effect of flow rate or residence time

The effect of flow rate (5–100 sccm) on the CF_2 density was examined at constant power (20 W), feed gas composition (25% CF_4/Ar), and pressure (66.7 Pa). In varying the flow rate over 5–100 sccm, the residence time for the gas within the volume between the electrodes was decreased from ~ 1.5 to ~ 0.07 s (nominal residence time=pressure $\times$volume/flow rate). Representative contour plots of the $[CF_2]$ at flow rates of 5, 18, and 100 sccm are shown in Fig. 6. These different flow rates resulted in relatively minor changes in the spatial distribution of CF_2 as illustrated by the similarity of the contours in Fig. 6 and in the axially averaged ($0 < z < 1.2$ cm) radial profiles in Fig. 7(a). For example,
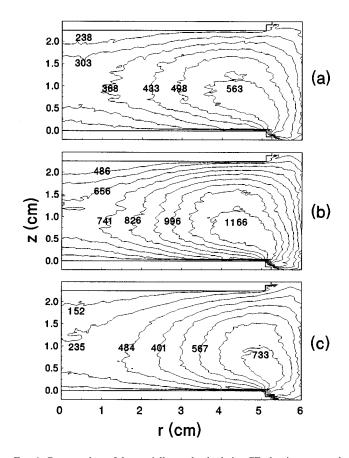

FIG. 6. Contour plots of the spatially resolved relative CF_2 density measured with laser-induced fluorescence in 25% CF_4/Ar, 66.7 Pa (500 mTorr), 20 W discharges at (a) 5, (b) 18, and (c) 100 sccm.

the normalized CF_2 density distribution was very similar for flow rates below 25 sccm ($\sigma \sim 21\%$), although at higher flows the edge-to-center uniformity was somewhat worse [$\sigma = 39\%$ at 100 sccm, see Fig. 7(a)], due to an enhancement in $[CF_2]$ near the edge of the discharge. The better uniformity at the lower flow rates may be due, in part, to enhanced diffusion with respect to convection.

Although the spatial distribution of CF_2 at the various flow rates was not dramatically affected, a significant nonmonotonic variation in the overall concentration was observed. This is evident in Fig. 7(b), where the image-averaged $[CF_2]$ is shown as a function of flow rate. At low flow rates (high residence time), the $[CF_2]$ initially increases with flow rate. Further increases in flow rate (shorter residence times) result in a subsequent decrease in $[CF_2]$. Because the CF_2 production rate likely remains essentially constant (the electron number density and temperature are approximately constant and the CF_4 is largely undissociated), these changes in $[CF_2]$ with flow rate suggest a competition among its various loss processes, which include convection, gas-phase recombination, surface losses, and diffusion.

While further modeling and experiments are necessary to be certain, this variation in $[CF_2]$ with flow rate might be explained as follows. At moderately high flow rates (i.e., 25 sccm) further increases in the flow rate yield a decrease in the accumulation of CF_2 within the discharge, because the
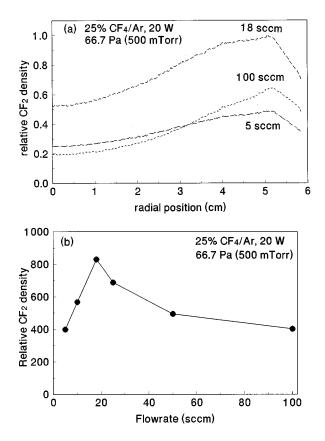
FIG. 7. (a) Axially averaged ($0<z<1.2$ cm) radial profiles of CF_2 density ($\sigma=22\%$, 21%, and 39% for 5, 18, 100 sccm, respectively) and (b) image-averaged CF_2 density as a function of flow rate, determined from PLIF images of 25%CF_4/Ar discharges at 66.7 Pa (500 mTorr) and 20 W.
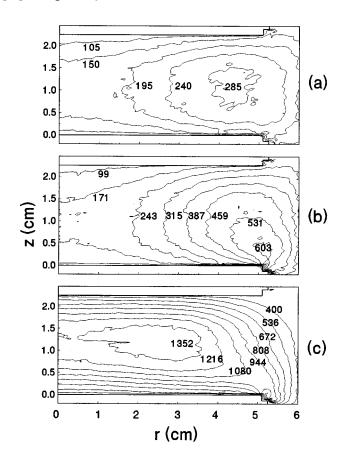

FIG. 8. Contour plots of the spatially resolved relative CF_2 density measured with laser-induced fluorescence in 75%CF_4/Ar, 10 sccm, 12 W discharges at (a) 13.3 Pa (100 mTorr), (b) 33.3 Pa (250 mTorr), and (c) 133.3 Pa (1000 mTorr).

dissociation products are convected away more rapidly. As the flow rate is reduced (from say 50 sccm), initially the $[CF_2]$ increases because of reduced convective losses. While convection becomes less important, the primary CF_2 gas-phase recombination reaction,[28] $CF_2+F+M\rightarrow CF_3+M$, becomes somewhat more important since the CF_2 (and F) concentration increases. The CF_2 surface losses also increase because diffusive transport becomes increasingly important at lower flow rates.

As the flow rate is further reduced (below $\sim$18 sccm), though, the observed decrease in $[CF_2]$ cannot be attributed to increased gas-phase recombination, because that rate only depends on the (decreasing) CF_2 and F concentration. Furthermore, the observed decrease in $[CF_2]$ below 18 sccm cannot be attributed to the temperature dependence of the fluorescence signal, because we expect the temperature to increase with decreasing flow rate (see below), which would lead to (slightly) systematically high $[CF_2]$ measurements at lower flow rates (see Sec. II above). Consequently, we (speculatively) attribute the observed decrease in $[CF_2]$ at very low flows to an increased loss due to diffusion, either by surface losses or by transport out of the imaged region. This increase in diffusional losses may result from an increase in the neutral gas temperature and, hence, diffusion coefficient (note that the diffusion coefficient $\propto T^{3/2}$).[2] Indeed, an increase in temperature is expected as the flow rate

is reduced, because, with constant rf power and a reduced enthalpy efflux, more thermal energy accumulates within the discharge. Such an increase in the contribution of diffusion and surface recombination reactions at low flow rates has been indicated in previous modeling of F-atom concentration in CF_4/O_2 plasmas.[31]

D. Effect of pressure

The effect of pressure on the $[CF_2]$ was examined at constant flow rate (10 sccm), composition (75% CF_4/Ar), and power (12 W), with pressures ranging from 13.3 to 133.3 Pa (100–1000 mTorr). Representative CF_2 spatial distributions are shown for three pressures in Fig. 8, and additional cases at 66.7 Pa (500 mTorr) are shown in figures above [e.g., Figs. 2 and 4(a)]. As noted previously, varying the pressure led to significant changes in both the magnitude and spatial distribution of CF_2 density.

Changes in the overall magnitude of $[CF_2]$ are illustrated in Fig. 9(a). For the conditions examined here, the image averaged $[CF_2]$ increases linearly with pressure with a *normalized* slope of $\sim$0.5, which is to some extent consistent with the results of Pang and Brueck;[12] they, however, observed a larger initial slope in pure CF_4 plasmas as well as a saturated CF_4 concentration above 66.7 Pa (500 mTorr). The present increase in $[CF_2]$ with pressure can be attributed to
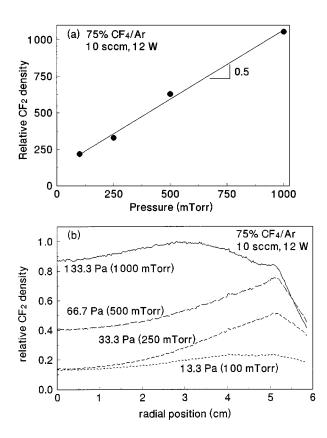
FIG. 9. (a) Image-averaged CF$_2$ density as a function of pressure in 75%CF$_4$/Ar, 10 sccm, 12 W discharges and (b) axially averaged ($0 < z < 1.2$ cm) radial profiles of CF$_2$ density (σ=22%, 45%, 21%, and 14% for 13.3, 33.3, 66.7, and 133.3 Pa, respectively). The normalized slope indicated in (a) denotes that the [CF$_2$] increases by 5× as the pressure is increased by 10×.

increased electron impact production of CF$_2$, because both the electron and CF$_4$ density are expected to increase with pressure. On the other hand, this relative weakness of the increase in [CF$_2$] (and thus CF$_4$ dissociation) with pressure may be due to the cooling of the high energy electron energy distribution at the higher pressures.

Figure 9(b) shows the axially averaged radial [CF$_2$] profiles as a function of pressure. The changes in these profiles with pressure are perhaps the most difficult to interpret, because they result from a complex interaction among the production, transport, and loss mechanisms of CF$_2$, including changes in the electron energy distribution, residence time, and rates of diffusion and gas-phase recombination. The understanding of these observed pressure dependent CF$_2$ distributions would clearly benefit from detailed modeling studies, but there are some interesting trends which are worth noting. For example, the profiles for the 13.3–66.7 Pa cases show a similar character with the peak [CF$_2$] near the edge of the electrode, while the profile at 133.3 Pa is substantially different, with the peak [CF$_2$] found closer to the center of the discharge. In varying the pressure, we also observe the largest changes in radial uniformity, with the poorest uniformity at 33.3 Pa (σ=45%) and the best at 133.3 Pa ($\sigma\sim$14%). This large change in uniformity occurs because as pressure is increased from 13.3 to 33.3 Pa, the [CF$_2$] primarily increases

TABLE I. Summary of plasma electrical measurements, including the peak-to-peak amplitudes of the as-measured voltage wave form (V_{rf}), the corrected fundamental peak-to-peak amplitudes of the voltage (V_{pe}) and current (I_{pe}) wave forms at the powered electrode, the phase difference between V_{pe} and I_{pe}, the dc self-bias voltage (V_{dc}), and the power deposited to the plasma.

CF$_4$+O$_2$ (%)[a]	Flow rate (sccm)	Pressure (Pa)	Power (W)	V_{rf} (V)	V_{pe} (V)	I_{pe} (A)	ϕ (deg)	$-V_{dc}$ (V)
75/0	25	66.7	3.5	150	164	0.262	−49.4	18
75/0	25	66.7	12	300	328	0.660	−63.4	57
75/0	25	66.7	35	600	657	1.290	−71.1	175
5/0	25	66.7	21	440	485	1.063	−71.4	151
75/0	25	66.7	20	440	481	0.968	−69.5	110
100/0	25	66.7	20	430	472	0.980	−69.4	114
75/5	25	66.7	20	285	314	0.956	−57.2	45
75/10	25	66.7	20	245	272	0.905	−48.6	25
25/0	5	66.7	20	423	464	0.928	−67.7	114
25/0	18	66.7	20	439	479	0.912	−68.5	122
25/0	100	66.7	20	452	495	0.910	−68.9	131
75/0	10	13.3	12	445	489	0.696	−73.5	199
75/0	10	33.3	12	351	383	0.667	−67.4	94
75/0	10	66.7	12	298	327	0.665	−63.5	59
75/0	10	133.3	12	230	253	0.529	−43.2	25

[a]Balance of mixture is argon.

near the edge of the discharge, while as pressure is increased from 33.3 to 133.3 Pa, the [CF$_2$] increases more substantially near the center of the discharge. As discussed below, a significant change in the plasma impedance is also observed over this pressure range, with the plasma becoming more resistive at higher pressures.

E. Electrical measurements

In addition to the [CF$_2$] measurements, voltage and current wave forms were measured near the base of the powered electrode to characterize the discharge and permit comparisons to model calculations and future experimental studies. Table I shows a compilation of the electrical measurement results, including the peak-to-peak amplitudes of the powered electrode voltage (V_{pe}) and current (I_{pe}) wave forms corrected for cell parasitics, the relative phase (ϕ) between the corrected voltage and current wave forms, the dc self-bias voltage (V_{dc}), and the power delivered to the plasma. As noted above, these data are derived from a Fourier analysis of the measured electrical wave forms using an equivalent circuit model of the GEC cell and the external circuitry.[20]

In comparing these electrical data to the CF$_2$ measurements detailed above, we observe that the cases with the most uniform radial distribution of CF$_2$ correspond to cases with the most resistive plasma impedances, i.e., the cases in which ϕ is closest to 0°. In particular, these include the cases with the lowest power (3.5 W), highest pressure (133.3 Pa), and highest O$_2$ concentration (10%). For these cases, ϕ ranges from −43 to −49° compared to the other cases where ϕ ranges from −57 to −73°. The increased uniformity for the more resistive cases may result from an increase in the production of CF$_2$ within the plasma bulk, compared to the production near the powered electrode sheath. This assertion is also supported by axial ($r=0$) profiles of the plasma emis-

sion images (not shown here) which show an enhancement of excitation within the bulk, relative to the powered sheath region.

As one might anticipate, we also find that the cases which show largest changes in the CF_2 spatial distribution also show the largest changes in I_{pe} and ϕ, and to a lesser extent V_{dc} and V_{pe}. For example, increasing the pressure from 66.7 to 133.3 Pa showed one of the largest relative changes in the electrical measurements (I_{pe} decreased 20%, ϕ increased 32%) and also showed the *largest* change in CF_2 spatial distribution (see Fig. 9). In addition, increasing the power from 3.5 to 35 W showed a large change in the electrical measurements (I_{pe} increased by 5×, ϕ decreased by 44%), a seven-fold increase in CF_2 density, and moderate changes in the CF_2 spatial distribution. In contrast, varying the CF_2 concentration from 5%–100% and varying the flowrate from 5–100 sccm led to very little change in either the electrical measurements or the CF_2 spatial distribution.

IV. CONCLUDING REMARKS

In this experimental study, we have used planar laser-induced fluorescence imaging to measure spatially resolved 2D maps of CF_2 density in low-pressure rf $Ar/CF_4/O_2$ discharges generated within a GEC reference cell. In general, we found that varying the pressure led to significant changes in both the magnitude and spatial distribution of CF_2 density, while varying the composition, flow rate, and power primarily only affected the magnitude of the CF_2 density, with more subtle changes in the spatial distribution. Typically, the centerline ($r=0$) axial CF_2 distribution was symmetric with the local peak occurring near the center of the electrode gap, but, in all cases, significant radial variations in CF_2 density were observed ($14 \leq \sigma \leq 45\%$) with the peak density occurring near the edge of the discharge region. The most uniform radial distributions were observed for the cases with the lowest power (3.5 W), highest pressure (133.3 Pa) and highest O_2 concentration (10%), which, based on the accompanying electrical measurements, were the cases with the most resistive plasma impedances.

Based on plots of the image-averaged CF_2 concentration, for the conditions examined here, the CF_2 density increased linearly with power and CF_4 mole fraction in Ar/CF_4 discharges; the dissociation fraction in mildly diluted CF_4 discharges was less than a few percent; and the CF_2 density decreased substantially with the addition of oxygen. In addition, the CF_2 density was also found to vary nonmonotonically with flow rate, which we attributed to changes in the various loss rates for CF_2, including increased convective losses at high flows and increased diffusive losses at low flow rates.

ACKNOWLEDGMENTS

[1]*Plasma Etching. An Introduction*, edited by D. M. Manos and D. L. Flamm (Academic, Boston, 1989).

[2]M. A. Lieberman and A. J. Lichtenberg, *Principles of Plasma Discharges and Materials Processing* (Wiley, New York, 1994).

[3]B. K. McMillin and M. R. Zachariah, J. Appl. Phys. **77**, 5538 (1995).

[4]B. K. McMillin and M. R. Zachariah, J. Appl. Phys. **79**, 77 (1996).

[5]P. J. Hargis, Jr., K. E. Greenberg, P. A. Miller, J. B. Gerardo, J. R. Torezynski, M. E. Riley, G. A. Hebner, J. R. Roberts, J. K. Olthoff, J. R. Whetstone, R. J. Van Brunt, M. A. Sobolewski, H. M. Anderson, M. P. Splichal, J. L. Mock, P. Bletzinger, A. Garscadden, R. A. Gottscho, G. Selwyn, M. Dalvie, J. E. Heidenreich, J. W. Butterbaugh, M. L. Brake, M. L. Passow, J. Pender, A. Lujan, M. E. Elta, D. B. Graves, H. H. Sawin, J. J. Kushner, J. T. Verdeyen, R. Horwath, and T. R. Turner, Rev. Sci. Instrum. **65**, 140 (1994).

[6]Y. Hikosaka and H. Sugai, Jpn. J. Appl. Phys. **32**, 3040 (1993); see also Y. Hikosaka, M. Nakamura, and H. Sugai, Jpn. J. Appl. Phys. **33**, 2157 (1994), and references therein.

[7]J. Wormhoudt, J. Vac. Sci. Technol. A **8**, 1722 (1990).

[8]H. C. Sun, V. Patel, E. A. Whittaker, B. Singh, and J. H. Thomas III, J. Vac. Sci. Technol. A **11**, 1193 (1993).

[9]K. Takahashi, M. Hori, and T. Goto, Jpn. J. Appl. Phys. **32**, L1088 (1993), and references therein.

[10]D. B. Oh, A. C. Stanton, H. M. Anderson, and M. P. Splichal, J. Vac. Sci. Technol. B **13**, 954 (1995).

[11]P. J. Hargis, Jr. and M. J. Kushner, Appl. Phys. Lett. **40**, 779 (1982).

[12]S. Pang and S. R. J. Brueck, Mater. Res. Soc. Symp. Proc. **17**, 161 (1983).

[13]Y. Matsumi, S. Toyoda, T. Hayashi, and M. Miyamura, J. Appl. Phys. **60**, 4102 (1986).

[14]K. Ninomiya, K. Suzuki, S. Nishimatsu, and O. Okada, J. Vac. Sci. Technol. A **4**, 1791 (1986).

[15]J. W. Thoman, Jr., K. Suzuki, S. H. Kable, and J. I. Steinfeld, J. Appl. Phys. **60**, 2775 (1986).

[16]J. P. Booth, G. Hancock, and N. D. Perry, Appl. Phys. Lett. **50**, 318 (1987); see also J. P. Booth, G. Hancock, N. D. Perry, and M. J. Toogood, J. Appl. Phys. **66**, 5251 (1989).

[17]M. Kitamura, H. Akiya, and T. Urisu, J. Vac. Sci. Technol. B **7**, 14 (1989).

[18]S. G. Hansen, G. Luckman, G. C. Nieman, and S. D. Colson, J. Appl. Phys. **68**, 2013 (1990), and references therein.

[19]L. D. B. Kiss, J.-P. Nicolai, W. T. Conner, and H. H. Sawin, J. Appl. Phys. **71**, 3186 (1992).

[20]M. A. Sobolewski, J. Vac. Sci. Technol. A **10**, 3550 (1992).

[21]B. L. Preppernau and T. A. Miller, in *Glow Discharge Spectroscopies*, edited by R. K. Marcus (Plenum, New York, 1993).

[22]R. K. Hanson, J. M. Seitzman, and P. H. Paul, Appl. Phys. B **50**, 441 (1990).

[23]D. S. King, P. K. Schenck, and J. C. Stephenson, J. Mol. Spectrosc. **78**, 1 (1979).

[24]W. Hack and W. Langel, J. Photochem. **21**, 105 (1983).

[25]W. Hack and A. Wilms, J. Phys. Chem. **90**, 4007 (1986).

[26]J. D. Jackson, *Classical Electrodynamics*, 2nd ed. (Wiley, New York, 1975).

[27]M. Surendra and C. R. Guarnieri, presented at the Workshop on Industrial Applications of Plasma Processing, 12th International Symp. on Plasma Chem., Aug. 21–25, Minneapolis, MN (1995).

[28]I. C. Plumb and K. R. Ryan, Plasma Chem. Plasma Proc. **6**, 205 (1986).

[29]K. Tachibana, Phys. Rev. A **34**, 1007 (1986).

[30]W. L. Morgan, Plasma Chem. Plasma Proc. **12**, 477 (1992).

[31]M. Dalvie and K. F. Jensen, J. Vac. Sci. Technol. A **8**, 1648 (1990).